High-Efficiency Organic Solar Concentrators for Photovoltaics

Michael J. Currie, *et al.*

Science **321**, 226 (2008);
DOI: 10.1126/science.1158342

Science (print ISSN 0036-8075; online ISSN 1095-9203) is published weekly, except the last week in December, by the American Association for the Advancement of Science, 1200 New York Avenue NW, Washington, DC 20005.

21. D. C. Martin *et al.*, *Astrophys. J.* **619**, L1 (2005).
22. P. Morrissey *et al.*, *Astrophys. J. Supp. Ser.* **173**, 682 (2007).
23. N. Scoville *et al.*, *Astrophys. J. Supp. Ser.* **172**, 1 (2007).
24. M. A. Zamojski *et al.*, *Astrophys. J. Supp. Ser.* **172**, 468 (2007).
25. More details are available in the supporting material on *Science* Online.
26. S. W. Falk, W. D. Arnett, *Astrophys. J.* **180**, L65 (1973).
27. S. J. Smartt *et al.*, *Science* **303**, 499 (2004).
28. K.S. is supported by the Henry Skynner Junior Research Fellowship at Balliol College, Oxford. S.J. acknowledges support by the Science and Technology Facilities Council (STFC) and Global Jet Watch, C.W. and E.S.W. by STFC, and M.S. by the Royal Society. This work is supported by Acceleration and Basic research programs of Ministry of Science and Technology/Korean Science and Engineering Foundation to S.K.Y. We gratefully acknowledge use of data from the NASA GALEX satellite, the CFHT, the ESO VLT, the Gemini Observatory, and the Hubble Space Telescope.

Supporting Online Material
www.sciencemag.org/cgi/content/full/1160456/DC1
SOM Text
Figs. S1 to S4
Tables S1 to S4
References

13 May 2008; accepted 30 May 2008
Published online 12 June 2008;
10.1126/science.1160456
Include this information when citing this paper.

High-Efficiency Organic Solar Concentrators for Photovoltaics

Michael J. Currie,* Jonathan K. Mapel,* Timothy D. Heidel, Shalom Goffri, Marc A. Baldo†

The cost of photovoltaic power can be reduced with organic solar concentrators. These are planar waveguides with a thin-film organic coating on the face and inorganic solar cells attached to the edges. Light is absorbed by the coating and reemitted into waveguide modes for collection by the solar cells. We report single- and tandem-waveguide organic solar concentrators with quantum efficiencies exceeding 50% and projected power conversion efficiencies as high as 6.8%. The exploitation of near-field energy transfer, solid-state solvation, and phosphorescence enables 10-fold increases in the power obtained from photovoltaic cells, without the need for solar tracking.

Photovoltaic (PV) concentrators aim to increase the electrical power obtained from solar cells. Conventional solar concentrators track the Sun to generate high optical intensities, often by using large mobile mirrors that are expensive to deploy and maintain. Solar cells at the focal point of the mirrors must be cooled, and the entire assembly wastes space around the perimeter to avoid shadowing neighboring concentrators.

High optical concentration without excess heating in a stationary system can be achieved with a luminescent solar concentrator (LSC) (*1*–*5*). LSCs consist of a dye dispersed in a transparent waveguide. Incident light is absorbed by the dye and then reemitted into a waveguide mode. The energy difference between absorption and emission prevents reabsorption of light by the dye, isolating the concentrated photon population in the waveguide. In this way, LSCs can achieve high optical concentrations without solar tracking (*6*). Unfortunately, the performance of LSCs has been limited by self-absorption losses that restrict the maximum possible concentration factor. Here we describe an efficient variant of an LSC that mimics a four-level laser design and exhibits optical concentrations suitable for practical applications.

Typically, LSC dye molecules are cast into a transparent plastic sheet; however, we deposited a thin film of organic dye molecules onto glass. Our devices were fabricated with thermal evaporation, but solution processing could also be used. Precise control over the film composition allowed us to apply the recent advances of organic optoelectronics to LSCs, including Förster energy transfer (*7*), solid state solvation (*8*), and phosphorescence (*9*). We term the resulting devices organic solar concentrators (OSCs).

To obtain the highest power efficiencies, we constructed tandem OSCs (*2*). Incident solar radiation first encounters an OSC employing a short-wavelength dye. Longer wavelengths are transmitted through the first OSC and absorbed by a longer-wavelength dye in a second OSC (Fig. 1). Alternatively, solar radiation transmitted through the top OSC can be gathered by a bottom PV cell or used to heat water in a hybrid PV thermal system (*2*).

We quantify self-absorption losses in OSCs using the self-absorption ratio S, defined as the ratio of the absorption coefficients at the absorption and emission maxima. We examined two emissive dyes: 4-(dicyanomethylene)-2-*t-butyl*-6-(1,1,7,7-tetramethyljulolidyl-9-enyl)-4*H*-pyran (DCJTB) (*10*) and platinum tetraphenyltetrabenzoporphyrin [Pt(TPBP)] (*11*). As shown in Fig. 2A, S for a DCJTB-based OSC is ~80. DCJTB belongs to the dicyanomethylene (DCM) class of laser dyes and is characterized by large Stokes shifts and red emission with near-unity quantum efficiency. Batchelder *et al.* selected this class of dyes for solar-concentrator applications partly because of its high self-absorption ratio (*3*, *4*).

To reduce concentration quenching, DCJTB was doped (2% v/v) into the host material tris(8-hydroxyquinoline) aluminum (AlQ_3), which forms stable amorphous films. The resulting AlQ_3:DCJTB (2%) film was 5.7 μm thick with an absorbance of 1.1 absorbance units (au) at the DCJTB absorption peak. S is enhanced when AlQ_3 is used as the host. AlQ_3 provides a polar environment that stabilizes the highly polar DCJTB excited state. The effect is known as solid-state solvation, and it red-shifts the DCJTB photoluminescence (PL) (*8*).

Förster energy transfer was used to reduce the required concentration and hence the self-absorption of the emissive dye. For example, in the rubrene-based OSC of Fig. 2A, we used rubrene and DCJTB in a 30:1 ratio, the maximum possible without incurring significant concentration quenching in rubrene or incomplete Förster transfer to DCJTB. The resulting AlQ_3:rubrene (30%):DCJTB (1%) film was 1.6 μm thick with an absorbance of 1.2 au at the rubrene absorption peak. Förster energy transfer from rubrene to DCJTB increases the self-

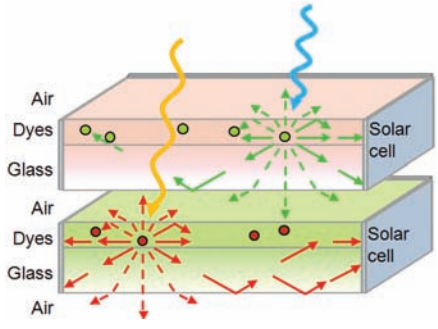

Fig. 1. Physical configuration of OSCs. (**Top**) OSCs consist of a thin film of organic dyes deposited on high-refractive-index glass substrates. The dyes absorb incident solar radiation and reemit it at a lower energy. Approximately 80% of the reemitted photons are trapped within the waveguide by total internal reflection for ultimate collection by a PV device mounted on the substrate edges. Photon loss (dashed lines) occurs because of nontrapped emission or absorption by other dyes. Blue arrow, high-energy incident visible light; green circles, dye molecules. (**Bottom**) Light transmitted through the first OSC can be captured and collected by a second OSC, whose dyes absorb and emit light at lower energies, for electrical conversion at a second, lower-bandgap PV device. Alternatively, the bottom OSC can be replaced by a low-cost PV cell or used to heat water in a hybrid PV thermal system. Yellow arrow, low-energy incident visible light; red circles, dye molecules.

Department of Electrical Engineering and Computer Science, Massachusetts Institute of Technology, Cambridge, MA 02139, USA.

*These authors contributed equally to this work.
†To whom correspondence should be addressed. E-mail: baldo@mit.edu

absorption ratio relative to the DCJTB-based OSC at the expense of narrower spectral coverage. However, rubrene is nonpolar and, together with a slight reduction in the DCJTB concentration, the DCJTB PL shifts ~20 nm back toward the blue.

Unlike DCJTB, which is fluorescent, Pt(TPBP) is phosphorescent. It emits from a weakly allowed triplet-state relaxation at wavelength (λ) = 770 nm with a PL efficiency of ~50% (*12*). As compared with conventional fluorescent dyes, an advantage of phosphorescent dyes is that the emissive state is only weakly absorptive. Thus, phosphors typically exhibit large Stokes shifts, eliminating the need for Förster transfer to a longer-wavelength emissive dye. *S* for the Pt(TPBP)-based OSC is ~500 (Fig. 2B). To fill the gap in the Pt(TPBP) absorption spectrum between λ = 430 and 610 nm, we added DCJTB, which efficiently transfers energy to Pt(TPBP). The resulting AlQ_3:DCJTB (2%):Pt(TPBP) (4%) film was 5.8 μm thick with an absorbance of 2.1 au at the Pt(TPBP) absorption peak. Förster energy transfer and phosphorescence are illustrated schematically in Fig. 2, C and D, respectively.

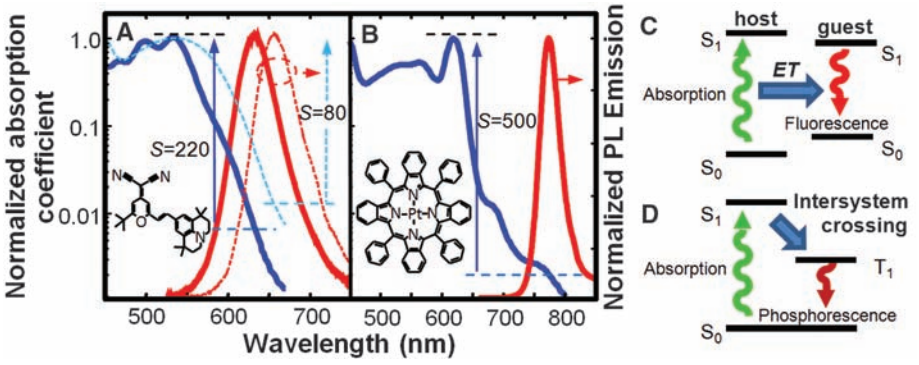

Fig. 2. Normalized absorption and emission spectra of OSC films. (**A**) The ratio between the peak absorption coefficient and the absorption coefficient at the emission wavelength provides an estimate of the self-absorption in an OSC film. In a DCJTB-based OSC, S = 80 (dotted lines). A larger ratio of S = 220 is obtained in a rubrene-based OSC (solid lines). S increases because the amount of DCJTB is reduced by a factor of 3. Its absorption is replaced by rubrene, which then transfers energy to DCJTB (C). The inset at left shows the DCJTB chemical structure. (**B**) Phosphorescence is another method to reduce self-absorption (D). In a Pt(TPBP)-based OSC, S = 500. The inset at left shows the Pt(TPBP) chemical structure. (**C**) Near-field dipole-dipole coupling known as Förster energy transfer can efficiently transfer energy between the dye donor and acceptor molecules. The concentration of guest molecules can be less than 1%, significantly reducing self-absorption. (**D**) Spin-orbit coupling in a phosphor increases the PL efficiency of the triplet state and the rate of intersystem crossing from singlet to triplet manifolds. The exchange splitting between singlet and triplet states is typically about 0.7 eV, significantly reducing self-absorption.

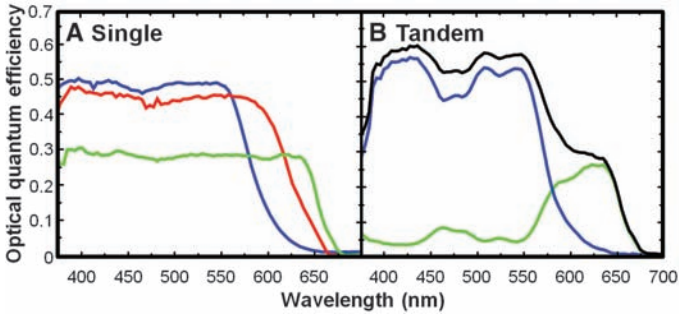

Fig. 3. OQE spectra at G = 3. The OQE is the fraction of incident photons that are emitted from the edges of the substrate. (**A**) The OQE spectra of the DCJTB- (red), rubrene- (blue), and Pt(TPBP)-based (green) single-waveguide OSCs. The DCJTB-based OSC is a 5.7-μm-thick film of 2% DCJTB in AlQ_3. The rubrene-based OSC is a 1.6-μm-thick film of 30% rubrene and 1% DCJTB in AlQ_3. The Pt(TPBP)-based OSC is a 5.9-μm-thick film of 2% DCJTB and 4% Pt(TPBP) in AlQ_3. (**B**) In the tandem configuration, light is incident first on the rubrene-based OSC (blue). This filters the incident light on the second, mirror-backed, Pt(TPBP)-based OSC (green). The composite OQE is shown in black.

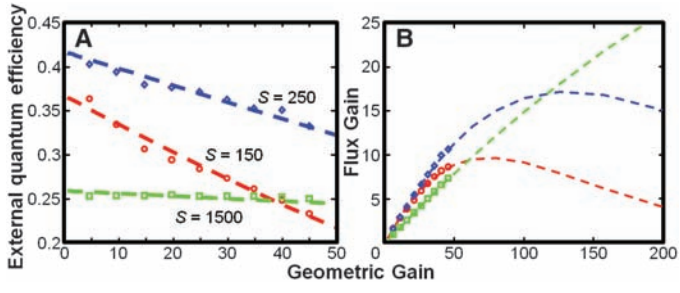

Fig. 4. OSC efficiency and flux gain as a function of geometric gain. (**A**) With increasing G, photons must take a longer path to the edge-attached PV, increasing the probability of self-absorption losses. The fit lines apply theory described in the SOM (*13*). (**B**) The flux gain is estimated based on the measured EQE (*13*). Flux gain increases with G but reaches a maximum when the benefit of additional G is cancelled by self-absorption losses. Near-field energy transfer (blue) and phosphorescence (green) substantially improve the flux gain relative to the DCJTB-based OSC (red). The dashed lines give the theoretical prediction for G > 50 based on the data for G < 50 (*13*).

The optical quantum efficiency (OQE), defined as the fraction of incident photons emitted from the edges of the OSC waveguides, was determined within an integrating sphere. The OQE is fundamentally limited by the product of the PL efficiency of the terminal dye and the fraction of photons that are emitted into waveguide modes (*13*). For an organic film refractive index of n = 1.7 au, and assuming photons are reemitted isotropically, ~80% of the photons are emitted into waveguide modes in the organic film or glass substrate (*2*). Waveguided photons not lost to self-absorption or scattering emerge from the edges of the OSC and are coupled to a PV cell. The remaining photons are emitted into the air through the top and bottom faces of the OSC. We distinguished between edge and facial emission by selectively blocking edge emission with ink and tape.

The ratio of the area of the concentrator to the area of the PV cell is the geometric gain G, also known as the geometric concentration factor. The OQEs of the single-waveguide OSCs at low geometric gain (G = 3, glass dimensions 25 by 25 by 2 mm, and n = 1.8 au) are compared in Fig. 3A. Higher-efficiency tandem OSCs were used with a rubrene-based OSC on top to collect blue and green light and the Pt(TPBP)-based OSC on the bottom to collect red light. Together, this tandem OSC combines higher-efficiency collection in the blue and green with lower-efficiency performance further into the red, as shown in Fig. 3B. At G = 3, the self-absorption is negligible, and the ratio of OQE between the DCJTB- and Pt(TPBP)-based devices approximately matches the ratio of their PL efficiencies (*13*).

The external quantum efficiency (EQE) is the number of harvested electrons per incident photon and includes all optical losses as well as the coupling losses at the PV interface and the quantum efficiency of the PV. The OSC films are evaporated onto a 100 by 100 by 1 mm SF10 glass substrate with a crystalline silicon PV attached along a single edge with optical epoxy. We measured EQE(G) by sweeping a point excitation normal to the detection edge while

monitoring the photocurrent (*13*). Figure 4A shows EQE(G) for each of the films, measured at λ = 534 nm for the fluorescent systems and λ = 620 nm for the phosphorescent system. The DCJTB-based OSC showed the strongest self-absorption. The self-absorption was lower in the rubrene-based OSC, which is consistent with the spectroscopic data in Fig. 2A. Finally, the Pt(TPBP)-based OSC showed no observable self-absorption loss for G < 50. The data matches the theoretical performance (*3*, *4*), assuming S = 150, S = 250, and S = 1500, for DCJTB-, rubrene-, and Pt(TPBP)-based OSCs, respectively (*13*).

Power-conversion efficiencies were estimated by integrating the product of the OQE, the AM1.5G spectrum (the standard spectrum of sunlight at Earth's surface), and solar-cell EQE weighted by the emission spectrum of each film (*13*). OSCs with emission from DCJTB were paired with GaInP solar cells (*14*); those with emission from Pt(TPBP) were paired with GaAs (*15*). The resulting power-conversion efficiencies are listed in Table 1. The estimated efficiency of the tandem OSC peaks at 6.8%.

We also calculated the power efficiency of tandem systems consisting of a top rubrene-based OSC whose transmission is incident on a CdTe or Cu(In,Ga)Se_2 (CIGS) PV cell (*16*, *17*). The OSC is predicted to increase the efficiency of CdTe and CIGS cells from 9.6 and 13.1% to 11.9 and 14.5%, respectively. There is a substantial opportunity to improve OSC efficiencies. The PL efficiency of the emissive dye can be increased, solar cells can be optimized for monochromatic and bifacial excitation, and the absorption spectrum should be expanded into the near infrared. With these advances, the power efficiency of tandem OSCs may exceed 20% (*2*).

Device stability in early LSC demonstrations was frustrated by the absence of photo-stable dyes (*4*). Since the original LSC studies, advances in dye-molecule design and packaging have yielded substantial progress in organic light-emitting diode (OLED) stability. In accelerated OLED stress tests, DCJTB and Pt(TPBP) have demonstrated stabilities exceeding 100 and 10 years, respectively (*11*, *18*). We have conducted preliminary stability measurements on our Pt(TPBP)-based OSCs using accelerated testing under an Oriel solar simulator with irradiance of 0.78 W/cm^2. The temperature of the OSC was 60°C. We observed that the PL efficiency of a 4% Pt(TPBP)-in-AlQ_3 sample decreased by 8% as compared with a dark-aged sample after the equivalent of 3 months outside (*13*). We expect that OSC lifetimes will approach the OLED standards when packaged and protected by ultraviolet filters.

The cost of a PV concentrator measured in cost per peak watt generated, $(\$/W_p)_{conc}$, is determined by its flux gain F, which is equal to the geometric gain after being corrected for efficiency losses in the concentrator; that is, $F = G\eta_{conc}/\eta_{PV}$ and

$$(\$/W_p)_{conc} = \frac{\text{collector cost}}{\eta_{conc} L} + \frac{1}{F}(\$/W_p)_{PV} \quad (1)$$

where L is the solar intensity, $(\$/W_p)_{PV}$ is the cost of the PV cell, and the power efficiencies of the concentrator and PV are η_{conc} and η_{PV}, respectively (*3*, *4*).

To compete with conventional power generation, $(\$/W_p)_{conc}$ must be <$\$1/W_p$. At mature production scales, we estimate that GaInP PV cells attached to the OSC will cost at least $\$50/W_p$ (*13*). Thus, the cost model yields a threshold value of $F \approx 50$. Equation 1 also shows that η_{conc} should be maximized to offset the collector cost. Previous LSC demonstrations yielded F < 5 with η_{conc} = 1.3% for the DCM class of laser dyes (*4*). In Fig. 4B and Table 1, we compare F for the three OSCs coupled to bandgap-matched solar cells. Based on measurements of OQE and EQE(G), we calculated F = 11 and η_{conc} = 4.7% for the rubrene-based OSC at G = 45. We extend the theoretical fit of OQE versus G to project performance at high geometric gain and predict a peak of F = 17 ± 2 for the rubrene-based OSC and F = 46 ± 15 for the Pt(TPBP)-based OSC.

OSCs aim to exploit high-performance PV cells in low-cost, nontracking solar concentrators. By using near-field energy transfer, solid-state solvation, and phosphorescence in thin-film organic coatings, we report OSCs that reduce the effective cost of inorganic solar cells by at least an order of magnitude. Combined with the potential for low-cost solution processing, the high flux gains and power efficiencies realized here should reduce the cost of solar power.

Table 1. Calculated power efficiency and flux gain of OSCs. The OSC parameters of OQE and spectral coverage were measured as a function of G. To project the performance of OSCs in combination with various solar cells, we calculated estimates of the power conversion efficiency of the combined systems (*13*). These calculations may underestimate the actual efficiencies by ignoring the benefits of optical concentration on the solar-cell open-circuit voltage and the ability to tailor solar-cell performance to narrow-band excitation. OSCs using energy transfer or phosphorescence best preserve power efficiency at high optical concentration (high G). However, both processes yield slightly lower performance at low G. Energy transfer decreases spectral coverage, and phosphorescence decreases the potential open-circuit voltage in the attached solar cell. The highest efficiencies are obtained from tandem structures: either combinations of rubrene- and Pt(TPBP)-based OSCs, or combinations of the rubrene-based OSC with CdTe or CIGS PV cells. The baseline efficiencies of the production CdTe and CIGS cells are 9.6 and 13.1%, respectively (*16*, *17*). SSS, solid state solvation; ET, energy transfer; Phos, phosphorescence; dash, not applicable.

Terminal absorber	Emitter	Processes	Power conversion efficiency at G = 3, 45	Flux gain at G = 45	Projected maximum flux gain
DCJTB	DCJTB	SSS	5.9%, 4.0%	9	12 ± 2 at G = 80
Rubrene	DCJTB	ET	5.5%, 4.7%	11	17 ± 2 at G = 125
Pt(TPBP)	Pt(TPBP)	Phos	4.1%, 4.1%	7	46 ± 15 at G = 630
Tandem: rubrene/Pt(TPBP)	DCJTB/Pt(TPBP)	ET/Phos	6.8%, 6.1%	—	—
Tandem: rubrene/CdTe PV	DCJTB	ET	11.9%, 11.1%	11	17 at G = 125
Tandem: rubrene/CIGS PV	DCJTB	ET	14.5%, 13.8%	11	17 at G = 125

References and Notes

1. W. H. Weber, J. Lambe, *Appl. Opt.* **15**, 2299 (1976).
2. A. Goetzberger, W. Greubel, *Appl. Phys. (Berlin)* **14**, 123 (1977).
3. J. S. Batchelder, A. H. Zewail, T. Cole, *Appl. Opt.* **18**, 3090 (1979).
4. J. S. Batchelder, A. H. Zewail, T. Cole, *Appl. Opt.* **20**, 3733 (1981).
5. K. Barnham, J. L. Marques, J. Hassard, P. O'Brien, *Appl. Phys. Lett.* **76**, 1197 (2000).
6. G. Smestad, H. Ries, R. Winston, E. Yablonovitch, *Sol. Energy Mater.* **21**, 99 (1990).
7. T. Förster, *Discuss. Faraday Soc.* **27**, 7 (1959).
8. V. Bulovic *et al.*, *Chem. Phys. Lett.* **287**, 455 (1998).
9. M. A. Baldo *et al.*, *Nature* **395**, 151 (1998).
10. J. Shi, C. W. Tang, *Appl. Phys. Lett.* **70**, 1665 (1997).
11. M. Thompson, *Mater. Res. Soc. Bull.* **32**, 694 (2007).
12. C. Borek *et al.*, *Angew. Chem. Int. Ed.* **46**, 1109 (2007).
13. See the supporting online material available on *Science* Online.
14. C. Baur *et al.*, *J. Sol. Energy Eng.* **129**, 258 (2007).
15. R. P. Gale *et al.*, paper presented at the 21st Institute of Electrical and Electronics Engineers (IEEE) Photovoltaic Specialists Conference, Kissimimee, FL, 1990.
16. S. H. Demtsu, J. R. Sites, paper presented at the 31st IEEE Photovoltaic Specialists Conference, Cape Canaveral, FL, 2005.
17. J. Palm *et al.*, *Thin Solid Films* **451-452**, 544 (2004).
18. V. V. Jarikov, D. Y. Kondakov, C. T. Brown, *J. Appl. Phys.* **102**, 104908 (2007).

19. This work was funded by the U.S. Department of Energy under grant DE-FG02-07ER46474 and NSF under grant OR 5653-001.01.

Supporting Online Material

www.sciencemag.org/cgi/content/full/321/5886/226/DC1
Tables S1 and S2
References

27 March 2008; accepted 9 June 2008
10.1126/science.1158342